

Design and Optimization of a Joined-Wing Aircraft

Andrew Bell, Josh Fromm, Scott Lowery, Spencer Riggs, Barret Sleeper, Michelle Tamayo, Jonathan Todd
and Oleg Usmanov
University of Colorado, Boulder, Colorado, 80309

The American Institute for Aeronautics and Astronautics (AIAA) hosts the annual Design, Build and Fly (DBF) competition. Teams of students from universities around the world compete to engineer a radio-controlled aircraft capable of successfully completing the mission designated by AIAA for that year. The 2007-2008 season required that the aircraft must be able to take off in 75 feet and have a wingspan no greater than 5 feet. Since the aircraft must also carry a significant payload, a crucial engineering challenge arose for designing an aircraft which has a short ground run, small wings and a high-lift capacity. The team from the University of Colorado at Boulder determined that the best design for this mission was a joined-wing configuration, in which there are two separate sets of wings that are connected to each other. This paper provides an overview of the processes involved in determining the span, planform area, incidence, dihedral and sweep of the wings. The final design allows for high efficiency in a compact package. The two wings produce an interference effect that bolsters the lift generated, produces outstanding stall characteristics and is also quite stable.

Nomenclature

AR	=wing aspect ratio	r	=vortex moment arm
b	=wing span	S	=wing planform area
C_{D0}	=coefficient of zero drag	V	=velocity
C_{Lmax}	=coefficient of maximum lift	W/S	=wing loading
e	=Oswald's efficiency factor	Γ	=vortex strength
g	=acceleration due to gravity	ρ	=air density
n	=load factor	$\Delta w/v$	=downwash angle
q	=dynamic pressure		

I. Introduction

The aerodynamic configuration of the aircraft consists of two main lifting surfaces: the upper forward wing which is swept back and the lower aft wing which is swept forward. The two wings are joined by vertical surfaces and there is no dedicated horizontal stabilizer. The large effective wing area promotes a high efficiency in terms of lift and wingspan, and the design can be both responsive and stable. However, this unorthodox approach to aircraft design presents certain difficulties when computing the appropriate geometry and stability matrices. The focus of this paper will be the procedure used for the determination and optimization of the wing geometry, its theoretical and experimental stall characteristics and an analysis of the dynamic stability.

II. Performance Constraints

A. Sizing Assumptions

For the preliminary sizing of the aircraft, a sizing constraint plot was created with a given set of assumptions. This plot is useful because the performance constraints can be written in terms of wing loading (W/S) and thrust loading (T/W). The combined constraint curves define a design region that meets all constraints. The following constraints were considered: takeoff distance, maneuvering, and stall speed. Table 1 illustrates the assumptions made in each sizing equation.

Table 1: Sizing Constraint Assumptions

Parameter	Assumed Value
Density Altitude (h_d)	6000 ft
Takeoff Weight (W_{TO})	15 lbs
Takeoff Distance (d_{TO})	70 ft
Load Factor (n)	2.5 G's
Stall Speed (V_{stall})	40 ft/s
Cruise Speed (V_{cruise})	70 ft/s

The density altitude is higher than that of Boulder by about 500 feet, introducing a margin of 8.33% and takeoff distance was set to 70 feet which provides for a 6.67% margin over the required 75 feet. The load factor of 2.5 G's is a competition requirement, and the plane was designed to meet this requirement during flight. The stall speed and cruise speeds were based on historical precedents for R/C aircraft, as were the 3-D effects on lift and the Oswald's efficiency factor.

B. Performance Equations and Chart

Equations (1) through (4) show the relationship between wing loading and thrust loading for each of the three constraints. Eq. (1), taken from [1], relates the wing loading and the thrust loading on takeoff, using the assumption that liftoff speed is 20% higher than the stall speed.

$$\text{Takeoff Constraint: } \frac{T_{static}}{W} = \frac{1.44}{g\rho C_{L_{max}} d_{TO} 0.8361} \left(\frac{W}{S}\right) \quad (1)$$

Acceleration due to gravity was set to a standard value of 32.2 ft/s² and the factor of 0.8361 represents propeller unloading when the aircraft begins moving. The three airfoils from the following section supplied the maximum lift coefficient ($C_{L_{max}}$), and a small 3-D correction factor of 0.2 was subtracted from these values. Differing coefficients of lift from each airfoil provides a method for understanding the variation of airfoil on overall aircraft design. The maneuvering constraint, Eq. (2), was found in [2].

$$\text{Maneuvering Constraint: } \left(\frac{T_{static}}{W}\right) = \left(\frac{1}{0.7}\right) \left(\frac{qC_{D_0}}{W} + \left(\frac{n^2}{q\pi AR e}\right) \left(\frac{W}{S}\right)\right) \quad (2)$$

The factor of 0.7 represents propeller unloading during flight and the zero-lift drag coefficient was taken from the airfoil data. The load factor (n) was assumed to be 2.5 G's, based on competition requirements. Oswald's efficiency factor is a measure of how efficiently the wings produce an elliptical lift distribution, and was assumed to be 0.8. The aspect ratio, as defined in Eq. (3) and found in [1], was computed using the maximum allowable dimension of 5 feet as the span and the area was computed from a range of wing loadings and a fixed takeoff weight, given in Table 1.

$$\text{Aspect Ratio: } AR = \frac{b^2}{S} \quad (3)$$

Eq. (4) was derived from the lift equation in [1], where $L = C_L q S$. The stall speed from Table 1 was selected based on nominal R/C aircraft values. Notice that thrust loading is not a factor in the stall speed constraint, meaning that stall provides a limiting factor on wing size:

$$\text{Stall Speed Constraint: } \frac{W}{S} = \frac{1}{2} \rho C_{L_{max}} V_s^2 \quad (4)$$

These three constraints were plotted for a range of wing loadings, from zero to 150 oz/ft²; these units are typically used for R/C aircraft. The plot is shown in Figure 1. The possible design region, shaded in orange, represents the area that meets the three constraints on the design. This region is bounded above by a thrust equal to the weight of the aircraft. The right bound is the stall speed of the aircraft and the lower bound is the maneuvering requirement of the aircraft. The takeoff requirement is not a bound on the design region. The star represents the optimal design point for the aircraft. This point maximizes wing loading and minimizes thrust loading, both of which minimize aircraft weight.

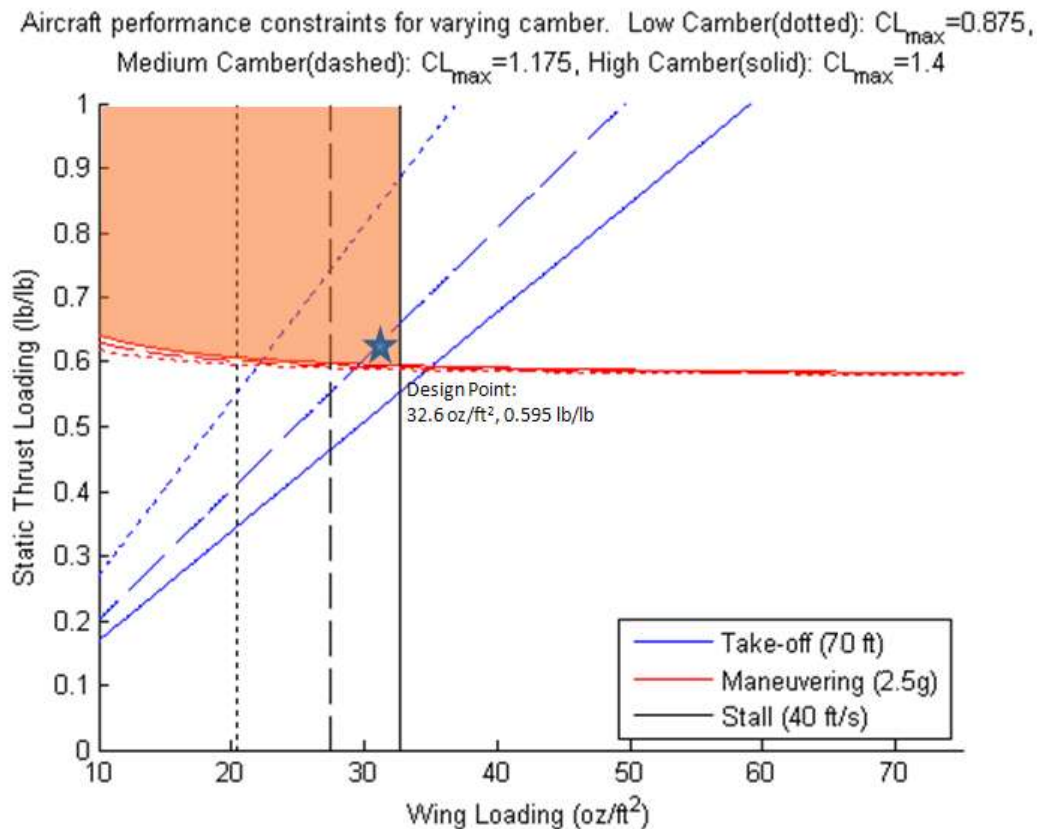


Figure 1: Performance Constraint Chart for Airfoils of Various Camber

The solid lines, representing the Eppler E216 airfoil, provide the highest wing loading and lowest thrust loading in the design region. Figure 1 assumes no high-lift devices being used on the aircraft. The ideal design point is a wing loading of 32.6 oz/ft² and a thrust loading of 0.595 lb/lb.

III. Airfoil Selection

The airfoil selection for the aircraft encompasses two main tasks: airfoil shape selection and airfoil incidence angle. The airfoil shape must be chosen before an incidence angle can be chosen. In order to choose an airfoil, the University of Illinois – Urbana-Champaign Airfoil Coordinates Database [3] was used in order to select a low-speed airfoil. This database contains hundreds of unique airfoils, and understanding each airfoil provides for the optimum design choice. The airfoils for propellers, sailplanes, turbines, and flying wings were immediately discarded because they are not designed for the flight profile of the aircraft. The remaining airfoils were analyzed at the design Reynolds number of 230,000 and compiled into a local database, named the Osborn database.

A. Profile Selection

The Osborn database was built by Matthew Osborn, a University of Colorado alumnus, for use in aircraft design projects. This database divides the viable airfoils into categories of low-, medium- and high-camber. The low-camber airfoils are distinguished by a camber of less than 4%; medium-camber is distinguished by a camber ratio between 4% and 6% and high-camber uses a camber ratio over 6%. From these families, the best airfoil is chosen based on post-stall behavior and its drag bucket. The Osborn database was built using XFOIL [4] to analyze each airfoil at a Reynolds number of 200,000. Osborn's analysis revealed that the best low-camber airfoil is the Eppler E226, the best medium-camber airfoil is the Selig-Ashok SA7036, and the best high-camber airfoil is the Eppler E216. The drag polars for these airfoils are shown in Figure 2 below.

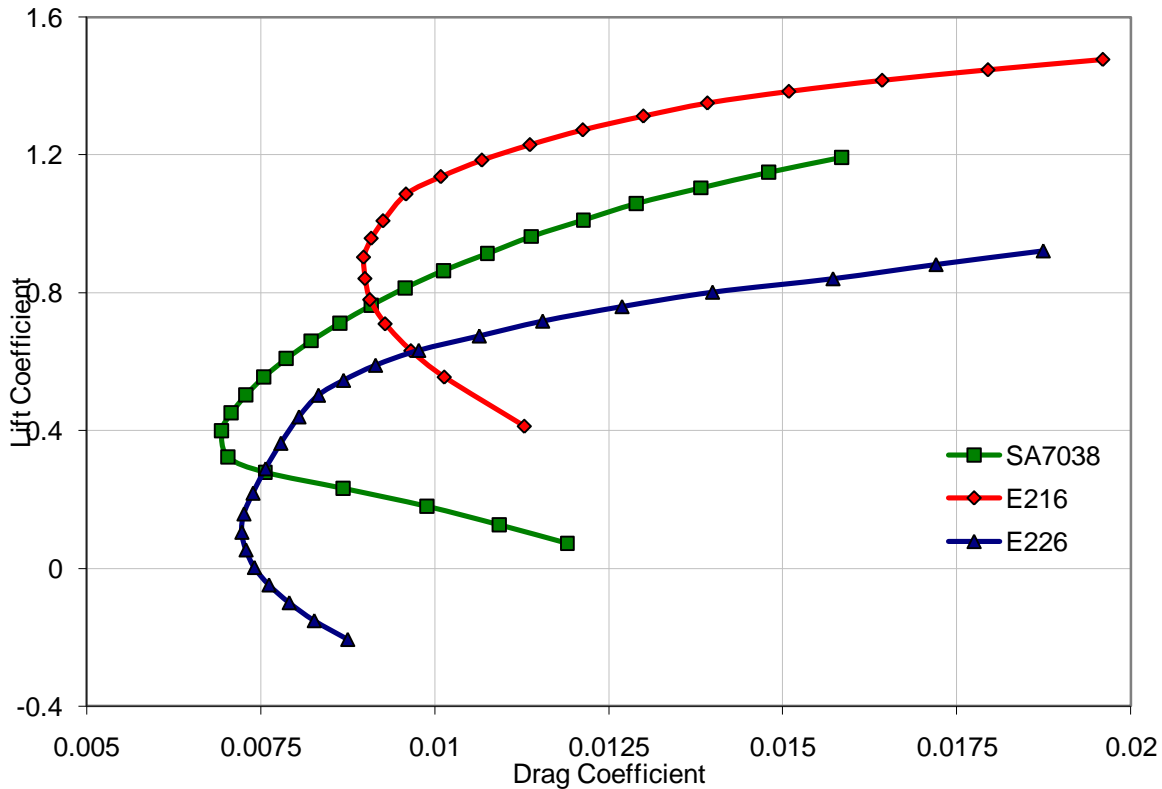


Figure 2: Final Airfoil Choice Drag Polars

The maximum lift coefficients of these airfoils were used to compute performance constraints in the previous section. There are three sets of three constraints; each set corresponds to an airfoil. The ideal airfoil choice provides for the highest wing loading and the lowest thrust loading; this provides the lowest system weight, which is desired. The airfoil that best meets this constraint, and was thus the final airfoil choice, is the Eppler E216 airfoil.

B. Incidence Angle

The next step of airfoil selection is to determine the incidence of the wings for the chosen airfoil. It was assumed that the fuselage is flying as close to zero angle of attack as possible to reduce drag. In order to analyze the airfoil properly, it was run in XFOIL at the design Reynolds number between the angles of -5° and 15° . The lift-slope curve is shown in Figure 3 along with an outline of the final airfoil selection.

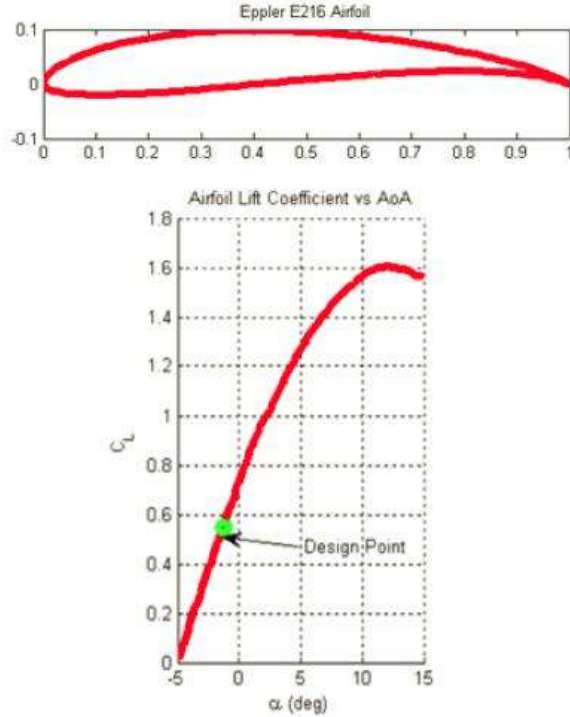


Figure 3: Eppler E216 Shape and Lift Curve

This provides a zero angle of attack close to expected cruise values and a very high angle of attack to stall the airfoil. The cruise lift coefficient was computed to be 0.37, which is a typical value for aircraft. This lift coefficient corresponds to an incidence angle of -1.2648° , which is not feasible for construction. The angle was rounded to the nearest tenth, which gives an angle of incidence of -1.3° . This is the design point shown in Figure 3 above.

IV. Geometric Design

A. Span Optimization

The first stage of the aerodynamic design was to determine the effects of varying the span. This analysis is crucial because at first glance, the span should be reduced as much as possible because a smaller span immediately provides several benefits. A smaller span reduces the overall weight of the aircraft and reduces the bending moment on the wings, as the length of the moment-arm is reduced. With these benefits of span reduction apparent, it is necessary to analyze other factors of aircraft performance in order to determine the negative effects of a smaller span.

The span optimization process is as follows. By keeping the total planform area of 9.58 ft^2 constant while the span was varied, the chords of both wings could be determined according to Eq. (5) below, in which this area is divided by the span:

$$c = \frac{S}{b} \quad (5)$$

The simplest gauge of an aircraft's effectiveness is the ratio between the lift and the drag, the L/D ratio. The greater the ratio, the more efficient the aircraft is. Using the MIT-developed Athena Vortex Lattice (AVL) [5] analysis tool, the L/D of the aircraft was computed for several different geometries. From the L/D, the total induced drag of the wing system was computed from Eq. (6):

$$D = \frac{w}{L} \frac{S}{D} \quad (6)$$

The wing loading, W/S, was determined from Figure 1. When multiplied by the aforementioned wing area, this value gives the weight of the aircraft which can be assumed to be equal to the lift as a common scenario. It should be noted that the L/D ratio used in this section gives only the induced drag by definition. Additionally, this procedure only accounts for the drag of the lifting surfaces, not the fuselage. This simplification is acceptable as only the performance of the wings is under question here; the fuselage drag may be assumed to be constant.

One last metric for gauging the effect of reducing the span is the power required to fly at cruise. Power is always given by a force times a velocity or, in this case, drag times the maximum cruise speed of 70 ft/s, as shown in Eq. (7).

$$P_{cruise} = DV \tag{7}$$

The results of the above three computations are summarized in Table 2.

Table 2: Span Optimization Results

Span (ft)	Chord of Forward Wing (ft)	Chord of Aft Wing (ft)	L/D	Induced Drag (lb)	Power at Cruise (W)
5	0.667	1.25	16.68	0.92	86.93
4.5	0.541	1.41	12.60	1.19	113.00
4	0.623	1.63	9.33	1.61	152.57

As is clear from Table 2, both the induced drag and the power increase as the span is decreased. This is a result of the efficiency, or L/D, of the aircraft decreasing. The results suggest that the span should be set to the maximum allowable value of 5 ft. However, does the decrease in weight compensate for the extra drag penalty? It was decided that the weight savings provided by reducing the span were negligible as the wings do not account for the majority of the final takeoff weight. Therefore, the optimal design is a span of 5 feet. Note that the chords used here are optimal values to be discussed in a later section.

B. Dihedral

Once the span has been determined, the next geometric parameter of the wings that was calculated was the dihedral angle. Negative dihedral, or anhedral, was eliminated from consideration due to concerns of ground clearance and takeoff rotation.

The goal of this analysis was to determine whether or not the typical dihedral-produced benefits of increased lateral stability apply to joined-wing aircraft. The effect of dihedral on stability was examined with the Dutch roll mode. The choice of this mode is due to the fact that rolling and yawing motion is coupled in this mode. For swept-wing aircraft such as this (sweep will be discussed in a later section), dihedral can cause dynamic instabilities. AVL was used to compute the roots of the Dutch roll mode under different angles of dihedral, which are shown in Table 3.

Table 3: Effect of Dihedral on Dutch roll

Aft Wing Dihedral	Dutch Roll Root
0 deg	0.11
2.5 deg	0.23
5 deg	0.35

Note that forward-wing dihedral was not considered due to propeller clearance concerns. The value shown in Table 3 is the real part of the root with positive values being unstable. This is true for all modes. The results make it clear that dihedral actually decreases the stability of this aircraft, and therefore will not be used.

C. Planform Area Distribution

Following the span optimization and the dihedral analysis, the next phase in the geometric design of the wings is the determination of how the total area should be distributed between the forward and aft wings. The goal of this analysis is to use the planform area distribution to set the neutral point of the aircraft as close to the ideal as possible.

The ideal neutral point (calculation of which is outside the scope of this paper) is 1.41 ft. aft of the root leading edge of the leading wing. Changing the percentage of area on each wing changes the aerodynamic center of the aircraft. Determining the appropriate distribution of the area is crucial because the only other way to change the neutral point is with wing sweep. As discussed in a later section, non-aerodynamic considerations limit the sweep to certain angles, and thus an adequate placement of the neutral point may not be possible with said limitations. From Eq. (5), the chords corresponding to each area distribution were computed. The AVL software was used to rapidly compute the various neutral points, and the results are shown in Table 4.

Table 4: Effect of Wing Area on Neutral Point

Percent of Area to Forward Wing	Chord of Forward Wing (ft)	Chord of Aft Wing (ft)	Neutral point (ft)
50	0.958	0.958	1.20
45	0.863	1.05	1.27
40	0.767	1.15	1.34
35	0.667	1.25	1.43

As is clear from Table 4, sizing the front wing to 35 percent of the total area sets the neutral point very close to its ideal value. This is fortunate as 35 percent area is close to the minimum area for the forward wing. Smaller areas bring the wing into the realm of a canard, in which it is used primarily for stability and not lift.

D. Wing Sweep

The last remaining geometric parameter necessary for the design of the wings is the sweep. The sweep angle of the forward wing was determined first, as it was limited by the system constraint of propeller clearance. Given the diameter of the propellers, the maximum allowable sweep angle was found using simple trigonometry to be 20 degrees.

The sweep of the rear wing must place the neutral point of the aircraft exactly at the desired value for longitudinal stability. As mentioned earlier, the ideal neutral point is 1.41 ft aft of the root chord leading edge of the forward wing. This value was used to compute the static margin of the aircraft. In order to ensure good flying qualities, there is a specific range to which the static margin must be set. For most aircraft this is typically five to fifteen percent. The greater the static margin, the more stable the aircraft is. Values less than five percent produce a “twitchy” aircraft that is difficult to control. Static margins substantially greater than fifteen percent produce a sluggish, unresponsive aircraft. For the DBF plane, it was assumed that the value should be on the upper side of the range, as the exact stability was unknown and because the various payloads will cause a slight c.g. shift which requires an additional margin.

The static margin was computed at a broad range of sweep angles, summarized in Table 5. Only integer values of the sweep angle were considered due to manufacturing tolerance concerns. As indicated by

the table, a forward sweep of 21 degrees yields the desired static margin of ten percent, plus extra to accommodate for the payload c.g. shift. Table 6 summarizes all of the important wing geometry components.

Table 5: Determination of Rear Wing Sweep

Rear Wing Forward Sweep Angle (deg)	CL_α	Cm_α	Computed Static Margin (%)	AVL Neutral Point (ft)	MAC (ft)
10	4.19	-0.96	22.91	1.50	0.73
15	4.18	-0.73	17.46	1.46	0.74
20	4.16	-0.5	12.02	1.42	0.73
21	4.14	-0.45	10.87	1.41	0.73
22	4.15	-0.4	9.64	1.40	0.73
23	4.15	-0.35	8.43	1.40	0.73
24	4.14	-0.3	7.25	1.39	0.73

Table 6: Final Wing Geometry

	Forward Wing	Aft Wing
Span	5 ft	5 ft
Chord	8 in	15 in
Area	3.33 ft ²	6.25 ft ²
Sweep	20 deg	-21 deg
Geometric Incidence	-1.3 deg	-1.3 deg
Dihedral	0 deg	0 deg

V. Stall Characteristics

A. Circulation and Downwash

The unique wing configuration of this aircraft promotes several excellent benefits in addition to span reduction. The positioning of the two wings allows for the circulation field around each wing to interfere with the other. Specifically, the rear wing induces an upwash on the forward wing, which in turn induces a

downwash on the rear wing. Since the rear wing is larger and produces the majority of the lift, its effect is greater, resulting on a net upwash over the aircraft. This effect is illustrated in Figure 4.

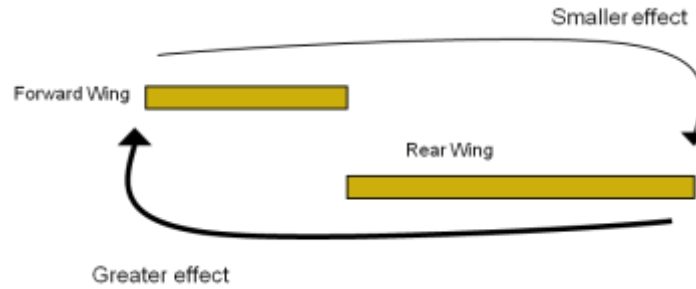


Figure 4: Side View Sketch of Circulation

This upwash changes the effective angle of attack that the front wing sees. The change can be calculated using a result from the Kutta-Joukowski theorem, shown in Eq. (8):

$$\left(\frac{\Delta w}{v}\right) = \frac{\Gamma}{2\pi Vc(r-0.25)} = \frac{C_L}{4\pi(r-0.25)}$$

$$\Gamma = \frac{1}{2} C_L Vc \tag{8}$$

In the above equation, r is the distance between the centers of the two wings; thus, the upwash varies along the span. The two extreme values are at the root and tip, in which the increase in angle of attack of the forward wing was found to be 0.03 and 0.10 degrees, respectively.

The increase in effective angle of attack has two benefits. First, it increases the overall lift available to the aircraft. More importantly, it improves the airplane’s stall characteristics. A higher angle of attack (and lower Reynolds number) on the front wing ensures that it always stalls first. This is crucial to the survival of the aircraft as a forward wing stall causes the nose of the aircraft to drop. On the other hand, a rear wing stall would send the plane into a tail-down spin, which reverses the airflow over the wing and control surfaces, a condition virtually guaranteed to be catastrophic. However, it has been shown that this will not occur. It should be noted the greater upwash at the tips is adverse, as tip stall causes the ailerons to lose functionality. However, since the aft wing, where the ailerons are located, are in downwash, a tip stall is unlikely to occur. If it became an issue, the span of the ailerons could be increased.

B. Test Results

A prototype of the aircraft was successfully flight-tested using the aforementioned geometry. During the test, the pilot brought the aircraft below the minimum stall speed. Instead of stalling, the aircraft tipped forward and recovered. This test was repeated several times with identical results. It can be deduced that the increased incidence seen by the forward wing influences this behavior and effectively negates stall speed requirements.

VI. Aircraft Stability

In order to determine the final stability of the aircraft, the geometry and airfoil previously discussed were inserted into AVL. Note that the aircraft does not have a vertical tail, and relies on lateral-directional stability from the vertical joiners. The stability derivatives were computed in AVL and inertias and masses were computed from a solid model built in CAD software. The longitudinal modes were defined from the eigenvalues of the longitudinal stability matrix, which is defined in Schmidt [6]. The eigenvalues correspond to the roots of the characteristic equation. These roots are plotted in the s-plane in Figure 5 below.

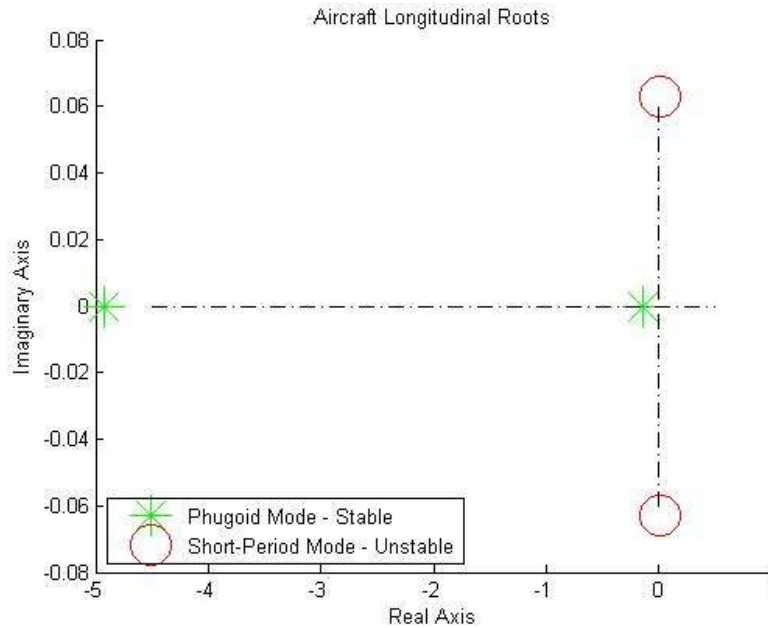


Figure 5: Longitudinal Eigenvalues

The longitudinal modes are rather unique for this aircraft. The phugoid mode does not demonstrate any oscillations; it disintegrates into two stable, damped roots. The short-period mode is slightly divergent, which is very rare in aircraft design. The instability in the short-period mode led the authors to construct a full-scale prototype aircraft from foam and wood. The prototype aircraft does exhibit this divergent behavior; however it is controllable without much effort, indicating that no design changes are needed.

The lateral-directional modes are also of great interest. The geometry in Figure 3 was analyzed for lateral-directional stability. Stability in these directions is determined by the eigenvalues of the lateral-directional stability matrix, also from Schmidt. The eigenvalues were plotted in the s-plane in Figure 6 to visually determine if the aircraft is passively stable in lateral-directional modes.

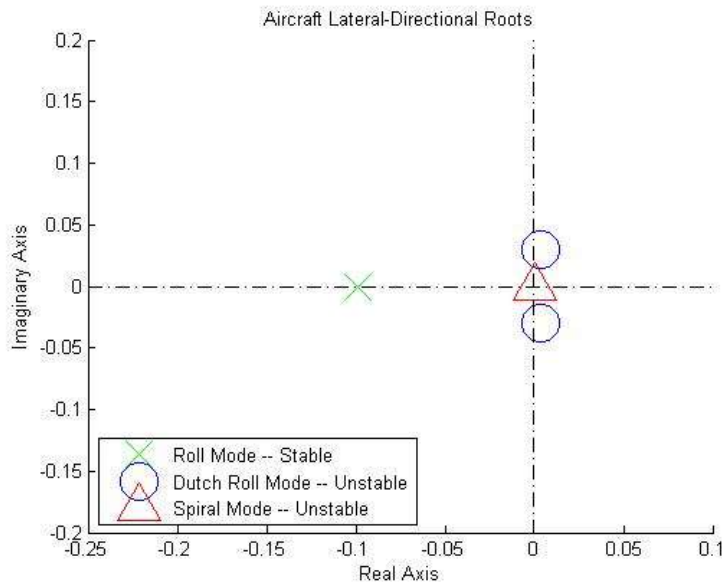


Figure 6: Lateral-Directional Eigenvalues without Vertical Tail

The spiral mode is neutrally stable, but the Dutch Roll mode is unstable from Figure 5. The addition of a vertical tail causes the Dutch Roll mode to become stable at the expense of the stability of the spiral mode. This was deemed an acceptable compromise as long as the spiral mode is slow and able to be controlled. The new lateral-directional eigenvalues are shown in Figure 7 below.

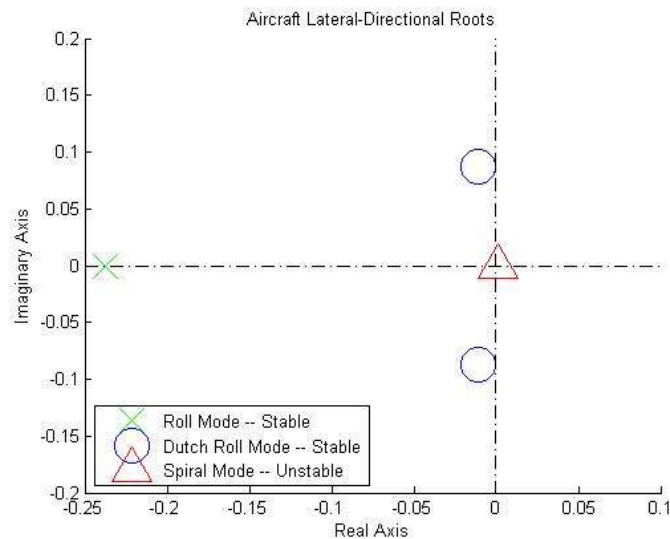


Figure 7: Final Lateral-Directional Eigenvalues

With the vertical tail, the Dutch roll mode is now stable and the spiral mode is unstable, but it is slow enough to be controlled. This stability was also seen during prototype test flying, with the aircraft exhibiting no major control problems in the lateral-directional modes. The vertical tail size was then varied to determine the influence of C_{np} , but even a slight change in the tail size caused a major decrease in the stability.

Joined-wing aircraft present unique challenges to computing stability and control derivatives when there is no dedicated horizontal tail. In order to satisfy all DBF mission constraints and performance objectives, the center of gravity of the aircraft must be in the center of the aircraft, which rules out the inclusion of a horizontal tail at the rear of the aircraft. All longitudinal control derivatives require the use of the lift-curve slope of the horizontal tail. Since this aircraft does not use a dedicated tail, the lift-curve slope of the pitch control surface is used, which is a more general term. In this case, the rear wing contains the pitch control surface, so its lift-curve slope would be used.

VII. Conclusions

Joined-wing aircraft are an unusual design choice for DBF, or any aircraft for that matter. They present unique challenges for determining optimal geometry and stability. It was found that utilizing the maximum allowable span maximizes the efficiency of the aircraft, and that the sweep of the wings plays a large role in the longitudinal stability of the aircraft. Additionally, it was found that due to their longitudinal proximity to the aircraft center of mass, the wing vertical joiners do not provide sufficient lateral-directional stability, and that a dedicated vertical tail is required. Once incorporated into the design, the aircraft is stable in most modes so as to be controllable without significant effort.

References

1. Shevell, Richard S. *Fundamentals of Flight*. 2nd ed. Upper Saddle River: Prentice Hall, 1989. 262-263.
2. Roskam, Jan. *Airplane Design Part I: Preliminary Sizing of Airplanes*. Lawrence, KS: DAR Corporation, 2003.
3. Selig, Michael. "UIUC Airfoil Coordinates Database." UIUC Airfoil Coordinates Database. 29 Nov. 2006. 1 Dec. 2007 <http://www.ae.uiuc.edu/m-selig/ads/coord_database.html>.
4. Drela, Mark. "XFOIL." Viscous Airfoil Solution Software. Massachusetts Institute of Technology.
5. Athena Vortex Lattice. Massachusetts Institute of Technology. Aerodynamic Analysis Software.
6. Schmidt, Louis V. *Introduction to Aircraft Flight Dynamics*. Reston: AIAA, 1998.